Article:

Thermou, G. orcid.org/0000-0002-9569-0176 and Hajirasouliha, I. (2018) Design-oriented models for concrete columns confined by steel-reinforced grout jackets. Construction and Building Materials, 178. pp. 313-326. ISSN 0950-0618

https://doi.org/10.1016/j.conbuildmat.2018.05.088

Design-Oriented Models for Concrete Columns Confined by Steel-Reinforced Grout Jackets

Georgia E. Thermou[1,2*] and Iman Hajirasouliha[1]

[1] Civil and Structural Engineering Department, The University of Sheffield, S1 3JD, Sheffield, UK
[2] Aristotle University of Thessaloniki, Dept. of Civil Engineering, 54124, Thessaloniki, Greece

Abstract: This paper investigates the axial stress–strain response of concrete confined with Steel-Reinforced Grout (SRG) jackets comprising of Ultra-High Tensile Strength Steel textiles embedded in an inorganic binder. Brittle, semi-ductile and ductile stress–strain response curves are identified according to the level of confinement stiffness provided by the SRG jackets. A comprehensive experimental database of 80 SRG-confined columns is developed and used to assess the influence of key design parameters. The results are then used to propose new design-oriented models to predict the strength and ultimate strain of SRG confined concrete columns by taking into account the confinement stiffness of the jackets.

Keywords: Confinement model; Concrete; Steel Fabric; Inorganic matrix; Mortar; SRG Jackets; Seismic strengthening.

[*]Corresponding author, tel: +44 (0) 114 222 5071, g.thermou@sheffield.ac.uk

1. Introduction

The use of externally-bonded composite reinforcement impregnated by resin is an efficient retrofit solution for accommodating deficiencies of existing reinforced concrete (RC) structures due to substandard detailing (e.g. sparse stirrup spacing, short lap splices) and ageing of the construction materials (e.g. steel corrosion). Fiber-Reinforced Polymer (FRP) jacketing is one of the most popular and widely used systems mainly due to the advantages such as not changing the geometry of retrofitted members, high-strength-to-weight ratio, corrosion resistance and relatively fast and easy application [e.g. 1-12]. However, the use of organic binders has some disadvantages such as high cost, toxicity, poor behaviour at high temperatures (low fire resistance), lack of vapour permeability and inapplicability on wet substrate or at low temperatures. The substitution of the organic binders with inorganic ones seems to minimize most of these drawbacks.

The first experimental studies demonstrated the effectiveness of carbon fiber sheets embedded in mortar matrix for the flexural strengthening of beams and confinement of concrete cylinders [13-16]. This led to a new generation of mortar-based composite systems, Fiber-Reinforced Cementitious Mortar (FRCM), where bidirectional textiles made of continuous composite fibers (i.e. carbon, glass, basalt, poliparafenilen benzobisoxazole (PBO)) are combined with mortars [e.g. 17-21]. Most of these composite systems have been used for confinement, flexural and shear strengthening of RC members.

In general, the success of a composite system relies on the bond developed between the composite fabric and the mortar. Therefore, the continuous fiber sheets used in FRP systems have been replaced by textiles which comprise bidirectional fabric meshes made of continuous woven or unwoven fiber rovings. The width of the rovings and their clear spacing define the density of the textile, which in turn controls the mechanical characteristics of the textile [17].

The degree of penetration of the mortar through the gaps between fiber rovings determines the quality of the interlock mechanism developed between the mortar and fabric [22-25].

Previous research studies towards the development of innovative and cost-effective retrofit solutions have led to the Steel-Reinforced Grout (SRG) system, where Ultra High Tensile Strength Steel (UHTSS) textiles are combined with inorganic binders for retrofitting of RC structures. The steel-reinforced fabrics comprise high strength unidirectional steel cords made by twisting filaments having a micro-fine brass or galvanized coating. The density of the steel fabric is defined by the distance between the cords. In a pilot study, Thermou and Pantazopoulou [22] investigated experimentally the confinement effectiveness of the SRG jackets applied to pre-damaged cantilever specimens with old type detailing. More recent studies highlighted the efficiency of the SRG jacketing in increasing both the compressive strength and the deformation capacity of confined concrete specimens [24, 26]. While the above studies demonstrated the efficiency of the SRG system for strengthening of RC columns, there is still no comprehensive research on the mechanical characteristics of steel cords and mortar mixes suitable for externally bonded reinforcement systems and the key parameters that affect their performance. Moreover, reliable and practical confinement models should be developed to predict the performance of SRG jacketed concrete specimens before this new system can be widely used in common practise.

In this paper the results of all available tests on SRG jacketed cylindrical concrete columns subjected to uniaxial compression are collected to create a comprehensive database. The adequacy of the existing FRP and FRCM confinement models is assessed by using the experimental database and it is shown that they cannot accurately predict the response of SRG confined concrete. The data is then used to develop a new design-oriented confinement model to predict the confined strength and ultimate strain of SRG-confined concrete. This is achieved by identifying the key design parameters and their impact on the axial stress-strain behaviour of SRG jacketed concrete specimens.

2. SRG jacketing method

Steel-Reinforced Grout jackets comprise Ultra High Tensile Strength Steel (UHTSS) fabrics combined with a mortar that serves as the connecting matrix. As shown in Fig. 1, the steel-reinforced fabrics are made of unidirectional steel cords (wires) fixed to a fibreglass micromesh to facilitate installation. The types of cords generally used are 12X (made by twisting 12 strands with over twisting of one wire around the bundle), 3X2 and 3X2* (made by wrapping three straight filaments by two filaments at a high twist angle) (see Fig. 1). Table 1 provides details regarding the geometrical and mechanical properties of the single cords as provided by the manufacturers. The 12X and 3X2 individual wires have a micro-fine brass coating to enhance their corrosion resistance. The 3X2* individual wires are galvanized, and therefore, have higher durability in a chloride, freeze-thaw and high humidity environment. The densities of the fabrics (i.e. cords per cm) examined in the previous studies by Thermou et al. [23] and Thermou and Hajirasouliha [26] were 1, 2, 9.06 cords/cm for the 12X and 3X2 fabrics and 1.57 and 4.72 cords/cm for the 3X2* fabric (see Fig. 1).

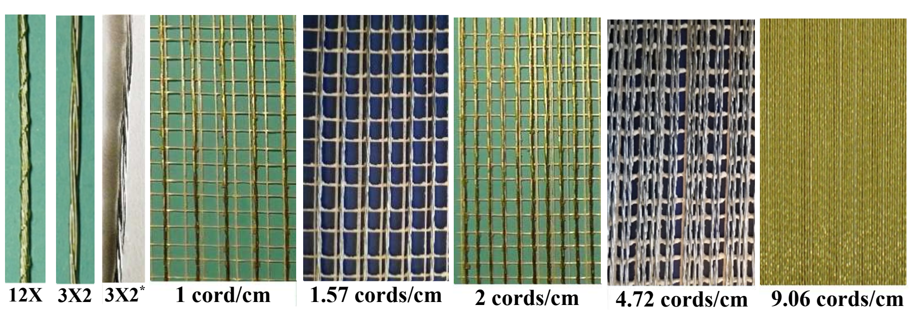

Figure 1: High strength steel cord types 12X, 3X2, 3X2* and Ultra High Tensile Strength Steel (UHTSS) textiles of 1, 1.57, 2, 4.72, 9.06 cords/cm density

The first step of the SRG application procedure involves the preparation of the substrate and the fabric. Unconfined cylindrical specimens should be cleaned and saturated with water before putting the first layer of the cementitious grout (usually with around 3 mm thickness). The fabrics are then cut into the desired lengths accounting for the number of layers and the overlap length. The fabrics with the density higher than 1 cord/cm are usually pre-bent to facilitate the wrapping process (Figs. 2a, b). The cementitious grout can be applied manually with the help of a trowel directly onto the lateral surface of the specimens (Fig. 2c). The steel fabric is placed immediately after the application of the cementitious grout (Figs. 2d, e). The grout is then squeezed out between the steel cords by applying pressure manually (Fig. 2f). After having placed one or two layers of fabric, the remaining length is lapped over the lateral surface. A final layer of the cementitious grout is then applied to the exposed surface (Fig. 2g). In the experimental tests conducted by Thermou et al. [23], the thickness of the grout layer including the steel reinforced fabric was 7 and 10 mm for one- and two-layered jackets, respectively, allowing the steel fabric to be fully embedded in the cementitious matrix.

Figure 2: Application procedure

It should be mentioned that, based on the Thermou et al. [23] and Thermou and Hajirasouliha [26] observations, using the 4.72 cords/cm fabric can impose some difficulties in the penetration of mortar through the small gaps, while in case of the 9.06 cords/cm fabric it is practically impossible. Additionally, handling of a dense fabric, even if it is pre-bent, can be very difficult due its high axial stiffness.

3. Experimental database

In this study, a comprehensive experimental database was compiled by gathering all the available tests on SRG jacketed cylindrical columns subjected to uniaxial compression [23, 26]. The database consists of 80 SRG-confined cylinders 150×300 mm. In general, the key design parameters in the experimental tests were the type and the density of the fabric, the number of layers, the overlap length, the mechanical characteristics of the inorganic matrix and the unconfined concrete strength.

In total 21 control cylindrical columns (150×300mm) used for measuring the concrete compressive strength of the different batches (3 cylindrical specimens for each group). Based on the concrete compressive strength of the unconfined concrete, f_{co}, which ranged between 15 and 30 MPa, 7 groups of specimens were identified in the experimental database. The variability of f_{co} in the database for SRG-confined concrete aimed to assess the impact of the unconfined concrete strength on the efficiency of the SRG system. One- and two-layered SRG jackets were applied, whereas three types of steel fabrics (12X, 3X2, 3X2*) with five different densities (1, 1.57, 2, 4.72, 9.06 cords/cm), three different overlap lengths (12, 24 and 36 cm) and four types of mortars (M1, M2, M3, M4) were examined.

Table 1 presents the details of the specimens and the utilised SRG jackets as well as the properties of the unconfined concrete, steel fabrics and mortars. For each specimen, the diameter of the high strength steel cords, D_{cord}, as well as the tensile strength, $f_{fu,s}$, and the strain at failure, $\varepsilon_{fu,s}$, of the textile are provided. In the case of mortar, the reported mechanical properties are the modulus of elasticity, E_m, the flexural strength, f_{mf}, and the adhesive bond strength, f_{mb}.

The first character of the identification code adopted (starting with A up to G) corresponds to the 7 groups explained above. The symbols “a”, “b” and “c” stand for 12X, 3X2 and 3X2* steel fabric, respectively. “L(i)” refers to the number of fabric layers with i=1 and 2 for one and two layers of the steel fabric, respectively. "D_j" identifies the density of the fabric with j=1, 2, 3, 4, 5 corresponding to 9.06, 4.72, 2, 1.57, 1 cords/cm, respectively. "M_k" refers to the type of inorganic matrix with k=1, 2, 3, 4 corresponding to mortars M_1, M_2, M_3, M_4. The symbols "s", "m" and "ℓ" correspond to an overlap length equal to 12, 24 and 36 cm, respectively. The number at the end of the identification code refers to the specimen number for each subgroup of the identical specimens. For example, CbL(1)D_5M_3ℓ_2 is the second specimen of Group C, where one layer of 3X2 steel fabric jacket with 1 cords/cm density was applied using the inorganic mortar M_3 and the overlap length of 36 cm.

Table 2 presents the test results including the compressive strength of unconfined concrete (f_{co}), the compressive strength of confined concrete (f_{cc}) and the corresponding strain (ε_{cc}), and the ultimate strain (ε_{ccu}) corresponding to 20% drop in the compressive strength of confined concrete ($0.80 \cdot f_{cc}$).

4. Experimental data analysis

4.1 Observed failure modes

The critical failure mode of SRG jacketing system is affected by the bond mechanism between the concrete substrate and the mortar, and also between the mortar and the steel cords. The SRG jacketing system is considered successful when rupture of the fabric occurs before mortar reaches its ultimate shear strength. The observed failure modes in the reference experimental tests were: (a) rupture of steel fabrics, (b) debonding, and (c) mixed mode of failure where debonding was followed by rupture of the steel fabric in a limited height of the specimen as shown in Fig. 3. Regarding the distribution of the failure modes in the experimental database, 31% of the specimens failed due to debonding (noted as D in Table 2), 9% exhibited a mixed mode of failure (noted as M in Table 2), whereas 60% failed due to rupture (noted as R in Table 2).

Table 1. Database on SRG confined concrete under axial loading – Details of the specimens

Ref.	No.	Specimen	Fabric							Mortar		
			Type	Density (cords/cm)	D_{cord} (mm)	Overlap length (mm)	No. of Layers	$f_{fu.s}$ (MPa)	$\varepsilon_{fu.s}$ (%)	E_m (GPa)	f_{mc} (MPa)	f_{mb} (MPa)
Thermou et al. [23]	1	AbL(1)D$_1$M$_1$s_1	3X2	9.06	0.889	360	1	2480	0.021	8.03	22.1	1.88
	2	AbL(1)D$_1$M$_1$s_2	3X2	9.06	0.889	360	1	2480	0.021	8.03	22.1	1.88
	3	AbL(1)D$_3$M$_1$s_1	3X2	2	0.889	360	1	2480	0.021	8.03	22.1	1.88
	4	AbL(1)D$_3$M$_1$s_2	3X2	2	0.889	360	1	2480	0.021	8.03	22.1	1.88
	5	AbL(1)D$_3$M$_1$s_3	3X2	2	0.889	360	1	2480	0.021	8.03	22.1	1.88
	6	AbL(1)D$_5$M$_1$s_1	3X2	1	0.889	360	1	2480	0.021	8.03	22.1	1.88
	7	AbL(1)D$_5$M$_1$s_2	3X2	1	0.889	360	1	2480	0.021	8.03	22.1	1.88
	8	AbL(1)D$_5$M$_1$s_3	3X2	1	0.889	360	1	2480	0.021	8.03	22.1	1.88
	9	AaL(1)D$_1$M$_1$s_1	12X	9.06	0.889	360	1	2014	0.019	8.03	22.1	1.88
	10	AaL(1)D$_1$M$_1$s_2	12X	9.06	0.889	360	1	2014	0.019	8.03	22.1	1.88
	11	AaL(1)D$_3$M$_1$s_1	12X	2	0.889	360	1	2014	0.019	8.03	22.1	1.88
	12	AaL(1)D$_3$M$_1$s_2	12X	2	0.889	360	1	2014	0.019	8.03	22.1	1.88
	13	AaL(1)D$_3$M$_1$s_3	12X	2	0.889	360	1	2014	0.019	8.03	22.1	1.88
	14	AaL(1)D$_5$M$_1$s_1	12X	1	0.889	360	1	2014	0.019	8.03	22.1	1.88
	15	AaL(1)D$_5$M$_1$s_2	12X	1	0.889	360	1	2014	0.019	8.03	22.1	1.88
	16	AaL(1)D$_5$M$_1$s_3	12X	1	0.889	360	1	2014	0.019	8.03	22.1	1.88
	17	BbL(1)D$_3$M$_1$ℓ_1	3X2	2	0.889	120	1	2480	0.021	8.03	22.1	1.88
	18	BbL(1)D$_3$M$_1$ℓ_2	3X2	2	0.889	120	1	2480	0.021	8.03	22.1	1.88
	19	BbL(1)D$_3$M$_1$ℓ_3	3X2	2	0.889	120	1	2480	0.021	8.03	22.1	1.88
	20	BbL(1)D$_5$M$_1$ℓ_1	3X2	1	0.889	120	1	2480	0.021	8.03	22.1	1.88
	21	BbL(1)D$_5$M$_1$ℓ_2	3X2	1	0.889	120	1	2480	0.021	8.03	22.1	1.88
	22	BbL(1)D$_5$M$_1$ℓ_3	3X2	1	0.889	120	1	2480	0.021	8.03	22.1	1.88
	23	BaL(1)D$_3$M$_1$ℓ_1	12X	2	0.889	120	1	2014	0.019	8.03	22.1	1.88
	24	BaL(1)D$_3$M$_1$ℓ_2	12X	2	0.889	120	1	2014	0.019	8.03	22.1	1.88
	25	BaL(1)D$_3$M$_1$ℓ_3	12X	2	0.889	120	1	2014	0.019	8.03	22.1	1.88
	26	BaL(1)D$_5$M$_1$ℓ_1	12X	1	0.889	120	1	2014	0.019	8.03	22.1	1.88
	27	BaL(1)D$_5$M$_1$ℓ_2	12X	1	0.889	120	1	2014	0.019	8.03	22.1	1.88
	28	BaL(1)D$_5$M$_1$ℓ_3	12X	1	0.889	120	1	2014	0.019	8.03	22.1	1.88
Thermou and Hajirasouliha [26]	29	CaL(1)D$_5$M$_1$ℓ_1	12X	1	0.889	360	1	2014	0.019	8.03	22.1	1.88
	30	CbL(1)D$_5$M$_1$ℓ_1	3X2	1	0.889	360	1	2480	0.021	8.03	22.1	1.88
	31	CbL(1)D$_5$M$_1$ℓ_2	3X2	1	0.889	360	1	2480	0.021	8.03	22.1	1.88
	32	CbL(2)D$_5$M$_1$ℓ_1	3X2	1	0.889	360	2	2480	0.021	8.03	22.1	1.88
	33	CbL(2)D$_5$M$_1$ℓ_2	3X2	1	0.889	360	2	2480	0.021	8.03	22.1	1.88
	34	CbL(2)D$_5$M$_1$ℓ_3	3X2	1	0.889	360	2	2480	0.021	8.03	22.1	1.88
	35	CaL(1)D$_5$M$_2$ℓ_1	12X	1	0.889	360	1	2014	0.019	10.35	4.01	2.94
	36	CbL(1)D$_5$M$_2$ℓ_1	3X2	1	0.889	360	1	2480	0.021	10.35	4.01	2.94
	37	CbL(1)D$_5$M$_2$ℓ_2	3X2	1	0.889	360	1	2480	0.021	10.35	4.01	2.94
	38	CbL(2)D$_5$M$_2$ℓ_1	3X2	1	0.889	360	2	2480	0.021	10.35	4.01	2.94
	39	CbL(2)D$_5$M$_2$ℓ_2	3X2	1	0.889	360	2	2480	0.021	10.35	4.01	2.94
	40	CbL(2)D$_5$M$_2$ℓ_3	3X2	1	0.889	360	2	2480	0.021	10.35	4.01	2.94
	41	CaL(1)D$_5$M$_3$ℓ_1	12X	1	0.889	360	1	2014	0.019	18.63	20.1	4.31
	42	CbL(1)D$_5$M$_3$ℓ_1	3X2	1	0.889	360	1	2480	0.021	18.63	20.1	4.31
	43	CbL(1)D$_5$M$_3$ℓ_2	3X2	1	0.889	360	1	2480	0.021	18.63	20.1	4.31
	44	CbL(2)D$_5$M$_3$ℓ_1	3X2	1	0.889	360	2	2480	0.021	18.63	20.1	4.31
	45	CbL(2)D$_5$M$_3$ℓ_2	3X2	1	0.889	360	2	2480	0.021	18.63	20.1	4.31
	46	CbL(2)D$_5$M$_3$ℓ_3	3X2	1	0.889	360	2	2480	0.021	18.63	20.1	4.31
	47	DaL(1)D$_5$M$_1$ℓ	12X	1	0.889	360	1	2014	0.019	8.03	22.1	1.88
	48	DaL(1)D$_5$M$_2$ℓ	12X	1	0.889	360	1	2014	0.019	10.35	4.01	2.94
	49	DaL(1)D5M$_3$ℓ	12X	1	0.889	360	1	2014	0.019	18.63	20.1	4.31

Table 1-cont. Database on SRG confined concrete under axial loading – Details of the specimens

Ref.	No.	Specimen	Fabric							Mortar		
			Type	Density (cords/cm)	D_{cord} (mm)	Overlap length (mm)	No. of Layers	$f_{fu.s}$ (MPa)	$\varepsilon_{fu.s}$ (%)	E_m (GPa)	f_{mc} (MPa)	f_{mb} (MPa)
Thermou and Hajirasouliha [26]	50	EcL(1)D_4M_4m_1	3X2*	1.57	0.827	240	1	2800	0.015	25.00	55.0	2.00
	51	EcL(1)D_4M_4m_2	3X2*	1.57	0.827	240	1	2800	0.015	25.00	55.0	2.00
	52	EcL(1)D_4M_4m_3	3X2*	1.57	0.827	240	1	2800	0.015	25.00	55.0	2.00
	53	EcL(1)D_4M_4ℓ _1	3X2*	1.57	0.827	360	1	2800	0.015	25.00	55.0	2.00
	54	EcL(1)D_4M_4ℓ _2	3X2*	1.57	0.827	360	1	2800	0.015	25.00	55.0	2.00
	55	EcL(2)D_4M_4m_1	3X2*	1.57	0.827	240	2	2800	0.015	25.00	55.0	2.00
	56	EcL(2)D_4M_4m _2	3X2*	1.57	0.827	240	2	2800	0.015	25.00	55.0	2.00
	57	EcL(2)D_4M_4ℓ _1	3X2*	1.57	0.827	360	2	2800	0.015	25.00	55.0	2.00
	58	EcL(2)D_4M_4ℓ_2	3X2*	1.57	0.827	360	2	2800	0.015	25.00	55.0	2.00
	59	FcL(1)D_4M_4ℓ_1	3X2*	1.57	0.827	360	1	2800	0.015	25.00	55.0	2.00
	60	FcL(1)D_4M_4ℓ_2	3X2*	1.57	0.827	360	1	2800	0.015	25.00	55.0	2.00
	61	FcL(1)D_4M_4ℓ_3	3X2*	1.57	0.827	360	1	2800	0.015	25.00	55.0	2.00
	62	FcL(2)D_4M_4m_1	3X2*	1.57	0.827	240	2	2800	0.015	25.00	55.0	2.00
	63	FcL(2)D_4M_4m_2	3X2*	1.57	0.827	240	2	2800	0.015	25.00	55.0	2.00
	64	FcL(2)D_4M_4m_3	3X2*	1.57	0.827	240	2	2800	0.015	25.00	55.0	2.00
	65	FcL(1)D_2M_4ℓ_1	3X2*	4.72	0.827	360	1	2800	0.015	25.00	55.0	2.00
	66	FcL(1)D_2M_4ℓ_2	3X2*	4.72	0.827	360	1	2800	0.015	25.00	55.0	2.00
	67	FcL(1)D_2M_4ℓ_3	3X2*	4.72	0.827	360	1	2800	0.015	25.00	55.0	2.00
	68	FcL(2)D_2M_4m_1	3X2*	4.72	0.827	240	2	2800	0.015	25.00	55.0	2.00
	69	FcL(2)D_2M_4m_2	3X2*	4.72	0.827	240	2	2800	0.015	25.00	55.0	2.00
	70	GcL(1)D_4M_4ℓ_1	3X2*	1.57	0.827	360	1	2800	0.015	25.00	55.0	2.00
	71	GcL(1)D_4M_4ℓ_2	3X2*	1.57	0.827	360	1	2800	0.015	25.00	55.0	2.00
	72	GcL(2)D_4M_4m_1	3X2*	1.57	0.827	240	2	2800	0.015	25.00	55.0	2.00
	73	GcL(2)D_4M_4m_2	3X2*	1.57	0.827	240	2	2800	0.015	25.00	55.0	2.00
	74	GcL(2)D_4M_4m_3	3X2*	1.57	0.827	240	2	2800	0.015	25.00	55.0	2.00
	75	GcL(1)D_2M_4ℓ_1	3X2*	4.72	0.827	360	1	2800	0.015	25.00	55.0	2.00
	76	GcL(1)D_2M_4ℓ_2	3X2*	4.72	0.827	360	1	2800	0.015	25.00	55.0	2.00
	77	GcL(1)D_2M_4ℓ_3	3X2*	4.72	0.827	360	1	2800	0.015	25.00	55.0	2.00
	78	GcL(2)D_2M_4m_1	3X2*	4.72	0.827	240	2	2800	0.015	25.00	55.0	2.00
	79	GcL(2)D_2M_4m_2	3X2*	4.72	0.827	240	2	2800	0.015	25.00	55.0	2.00
	80	GcL(2)D_2M_4m_3	3X2*	4.72	0.827	240	2	2800	0.015	25.00	55.0	2.00

Figure 3: SRG jacketed specimens failed due to (a) tensile fracture of the steel cords of the fabric; (b) mixed mode of failure; and (c) debonding

Table 2. Database on SRG confined concrete under axial loading – Experimental data

Ref.	No.	Specimen	f_{co} (MPa)	f_{cc} (MPa)	ε_{cc}	ε_{ccu}	f_{cc}/f_{co}	$\varepsilon_{ccu}/\varepsilon_{co}$	σ_{lat}/f_{co}	ρ_K	ρ_ε	Failure mode
Thermou et al. [23]	1	AbL(1)D_1M_1s_1	15.12	21.29	0.0047	0.0049	1.41	2.45	0.55	0.1190	4.6	D
	2	AbL(1)D_1M_1s_2		23.24	0.0052	0.0076	1.54	3.80	0.55	0.1190	4.6	D
	3	AbL(1)D_3M_1s_1		26.73	0.0083	0.0093	1.77	4.65	0.12	0.0263	4.6	R
	4	AbL(1)D_3M_1s_2		22.67	0.0033	0.0062	1.50	3.10	0.12	0.0263	4.6	D
	5	AbL(1)D_3M_1s_3		27.58	0.0088	0.0105	1.82	5.25	0.12	0.0263	4.6	R
	6	AbL(1)D_5M_1s_1		22.35	0.0055	0.0057	1.48	2.85	0.06	0.0131	4.6	R
	7	AbL(1)D_5M_1s_2		23.10	0.0044	0.0054	1.53	2.70	0.06	0.0131	4.6	R
	8	AbL(1)D_5M_1s_3		22.94	0.0058	0.0060	1.52	3.00	0.06	0.0131	4.6	R
	9	AaL(1)D_1M_1s_1		24.18	0.0041	0.0048	1.60	2.40	0.46	0.1091	4.2	D
	10	AaL(1)D_1M_1s_2		26.41	0.0044	0.0051	1.75	2.55	0.46	0.1091	4.2	D
	11	AaL(1)D_3M_1s_1		24.84	0.0058	0.0061	1.64	3.05	0.10	0.0241	4.2	D
	12	AaL(1)D_3M_1s_2		27.46	0.0062	0.0073	1.82	3.65	0.10	0.0241	4.2	R
	13	AaL(1)D_3M_1s_3		27.63	0.0077	0.0082	1.83	4.10	0.10	0.0241	4.2	D
	14	AaL(1)D_5M_1s_1		20.94	0.0037	0.0042	1.38	2.10	0.05	0.0120	4.2	R
	15	AaL(1)D_5M_1s_2		21.95	0.0034	0.0053	1.45	2.65	0.05	0.0120	4.2	R
	16	AaL(1)D_5M_1s_3		24.77	0.0037	0.0060	1.64	3.00	0.05	0.0120	4.2	R
	17	BbL(1)D_3M_1ℓ_1	26.20	31.47	0.0031	0.0047	1.20	2.35	0.07	0.0152	4.6	D
	18	BbL(1)D_3M_1ℓ_2		34.17	0.0031	0.0051	1.30	2.55	0.07	0.0152	4.6	D
	19	BbL(1)D_3M_1ℓ_3		42.57	0.0033	0.0051	1.62	2.55	0.07	0.0152	4.6	D
	20	BbL(1)D_5M_1ℓ_1		34.08	0.0027	0.0044	1.30	2.20	0.04	0.0076	4.6	D
	21	BbL(1)D_5M_1ℓ_2		37.86	0.0031	0.0040	1.45	2.00	0.04	0.0076	4.6	D
	22	BbL(1)D_5M_1ℓ_3		35.84	0.0028	0.0043	1.37	2.15	0.04	0.0076	4.6	R
	23	BaL(1)D_3M_1ℓ_1		42.99	0.0041	0.0054	1.64	2.70	0.06	0.0139	4.2	D
	24	BaL(1)D_3M_1ℓ_2		40.83	0.0030	0.0048	1.56	2.40	0.06	0.0139	4.2	D
	25	BaL(1)D_3M_1ℓ_3		37.43	0.0042	0.0058	1.43	2.90	0.06	0.0139	4.2	D
	26	BaL(1)D_5M_1ℓ_1		36.78	0.0026	0.0034	1.40	1.70	0.03	0.0069	4.2	R
	27	BaL(1)D_5M_1ℓ_2		37.90	0.0029	0.0033	1.45	1.65	0.03	0.0069	4.2	D
	28	BaL(1)D_5M_1ℓ_3		33.95	N/A	N/A	1.30	N/A	0.03	0.0069	4.2	R
Thermou and Hajirasouliha [26]	29	CaL(1)D_5M_1ℓ_1	23.14	28.75	0.0035	0.0069	1.24	3.45	0.03	0.0079	4.2	R
	30	CbL(1)D_5M_1ℓ_1		31.79	0.0038	0.0076	1.37	3.80	0.04	0.0086	4.6	R
	31	CbL(1)D_5M_1ℓ_2		32.81	0.0032	0.0066	1.42	3.30	0.04	0.0086	4.6	R
	32	CbL(2)D_5M_1ℓ_1		35.96	0.0080	0.0095	1.55	4.75	0.08	0.0172	4.6	R
	33	CbL(2)D_5M_1ℓ_2		40.61	0.0102	0.0106	1.75	5.30	0.08	0.0172	4.6	R
	34	CbL(2)D_5M_1ℓ_3		39.11	0.0104	0.0109	1.69	5.45	0.08	0.0172	4.6	R
	35	CaL(1)D_5M_2ℓ_1		29.80	0.0043	0.0058	1.29	2.90	0.03	0.0079	4.2	R
	36	CbL(1)D_5M_2ℓ_1		31.72	0.0034	0.0052	1.37	2.60	0.04	0.0086	4.6	R
	37	CbL(1)D_5M_2ℓ_2		28.51	0.0045	0.0093	1.23	4.65	0.04	0.0086	4.6	R
	38	CbL(2)D_5M_2ℓ_1		35.73	0.0068	0.0072	1.54	3.60	0.08	0.0172	4.6	R
	39	CbL(2)D_5M_2ℓ_2		31.56	0.0082	0.0087	1.36	4.35	0.08	0.0172	4.6	R
	40	CbL(2)D_5M_2ℓ_3		34.77	0.0067	0.0079	1.50	3.95	0.08	0.0172	4.6	R
	41	CaL(1)D_5M_3ℓ_1		33.07	0.0047	0.0059	1.43	2.95	0.03	0.0079	4.2	R
	42	CbL(1)D_5M_3ℓ_1		30.00	0.0046	0.0082	1.30	4.10	0.04	0.0086	4.6	R
	43	CbL(1)D_5M_3ℓ_2		34.30	0.0044	0.0069	1.48	3.45	0.04	0.0086	4.6	R
	44	CbL(2)D_5M_3ℓ_1		37.51	0.0080	0.0088	1.62	4.40	0.08	0.0172	4.6	R
	45	CbL(2)D_5M_3ℓ_2		40.39	0.0085	0.0089	1.75	4.45	0.08	0.0172	4.6	R
	46	CbL(2)D_5M_3ℓ_3		36.17	0.0074	0.0081	1.56	4.05	0.08	0.0172	4.6	R
	47	DaL(1)D_5M_1ℓ	16.62	30.45	0.0042	0.0069	1.83	3.45	0.05	0.0110	4.2	R
	48	DaL(1)D_5M_2ℓ		26.64	0.0049	0.0055	1.60	2.75	0.05	0.0110	4.2	R
	49	DaL(1)D5M_3ℓ		28.32	0.0056	0.0077	1.70	3.85	0.05	0.0110	4.2	R

Table 2-cont. Database on SRG confined concrete under axial loading – Experimental data

Ref.	No.	Specimen	f_{co} (MPa)	f_{cc} (MPa)	ε_{cc}	ε_{ccu}	f_{cc}/f_{co}	$\varepsilon_{ccu}/\varepsilon_{co}$	σ_{lat}/f_{co}	ρ_K	ρ_ε	Failure mode
Thermou and Hajirasouliha [26]	50	EcL(1)D$_4$M$_4$m_1	20.73	30.71	0.0066	0.0092	1.48	4.60	0.07	0.0206	3.3	D
	51	EcL(1)D$_4$M$_4$m_2		31.83	0.0097	0.0121	1.54	6.05	0.07	0.0206	3.3	D
	52	EcL(1)D$_4$M$_4$m_3		31.55	0.0051	0.0151	1.52	7.55	0.07	0.0206	3.3	D
	53	EcL(1)D$_4$M$_4$ℓ _1		33.82	0.0110	0.0111	1.63	5.55	0.07	0.0206	3.3	R
	54	EcL(1)D$_4$M$_4$ℓ _2		34.38	0.0079	0.0100	1.66	5.00	0.07	0.0206	3.3	R
	55	EcL(2)D$_4$M$_4$m_1		41.05	0.0088	0.0125	1.98	6.25	0.14	0.0412	3.3	R
	56	EcL(2)D$_4$M$_4$m _2		39.43	0.0120	0.0137	1.90	6.85	0.14	0.0412	3.3	R
	57	EcL(2)D$_4$M$_4$ℓ _1		42.66	0.0143	0.0163	2.06	8.15	0.14	0.0412	3.3	R
	58	EcL(2)D$_4$M$_4$ℓ_2		46.60	0.0104	0.0137	2.25	6.85	0.14	0.0412	3.3	R
	59	FcL(1)D$_4$M$_4$ℓ_1	18.27	27.53	0.0102	0.0112	1.51	5.60	0.08	0.0234	3.3	R
	60	FcL(1)D$_4$M$_4$ℓ_2		27.08	0.0035	0.0129	1.48	6.45	0.08	0.0234	3.3	M
	61	FcL(1)D$_4$M$_4$ℓ_3		28.42	0.0160	0.0168	1.56	8.40	0.08	0.0234	3.3	M
	62	FcL(2)D$_4$M$_4$m_1		34.99	0.0090	0.0149	1.92	7.45	0.15	0.0468	3.3	R
	63	FcL(2)D$_4$M$_4$m_2		36.33	0.0110	0.0130	1.99	6.50	0.15	0.0468	3.3	R
	64	FcL(2)D$_4$M$_4$m_3		38.00	0.0105	0.0110	2.08	5.50	0.15	0.0468	3.3	R
	65	FcL(1)D$_2$M$_4$ℓ_1		46.47	0.0150	0.0154	2.54	7.70	0.23	0.0703	3.3	D
	66	FcL(1)D$_2$M$_4$ℓ_2		40.56	0.0060	0.0060	2.22	3.00	0.23	0.0703	3.3	D
	67	FcL(1)D$_2$M$_4$ℓ_3		34.88	0.0060	0.0081	1.91	4.05	0.23	0.0703	3.3	D
	68	FcL(2)D$_2$M$_4$m_1		47.00	0.0120	0.0120	2.57	6.00	0.46	0.1406	3.3	M
	69	FcL(2)D$_2$M$_4$m_2		60.06	0.0230	0.0240	3.29	12.00	0.46	0.1406	3.3	M
	70	GcL(1)D$_4$M$_4$ℓ_1	29.98	40.90	0.0045	0.0133	1.36	6.65	0.05	0.0143	3.3	R
	71	GcL(1)D$_4$M$_4$ℓ_2		40.12	0.0024	N/A	1.34	N/A	0.05	0.0143	3.3	R
	72	GcL(2)D$_4$M$_4$m_1		44.58	0.0040	0.0112	1.49	5.60	0.09	0.0285	3.3	R
	73	GcL(2)D$_4$M$_4$m_2		46.25	0.0080	0.0133	1.54	6.65	0.09	0.0285	3.3	R
	74	GcL(2)D$_4$M$_4$m_3		44.80	0.0110	0.0124	1.49	6.20	0.09	0.0285	3.3	R
	75	GcL(1)D$_2$M$_4$ℓ_1		49.03	0.0045	0.0045	1.64	2.25	0.14	0.0428	3.3	D
	76	GcL(1)D$_2$M$_4$ℓ_2		46.02	0.0030	0.0084	1.54	4.20	0.14	0.0428	3.3	D
	77	GcL(1)D$_2$M$_4$ℓ_3		42.57	0.0065	0.0065	1.42	3.25	0.14	0.0428	3.3	D
	78	GcL(2)D$_2$M$_4$m_1		68.42	0.0112	0.0142	2.28	7.09	0.28	0.0857	3.3	M
	79	GcL(2)D$_2$M$_4$m_2		64.52	0.0090	0.0103	2.15	5.17	0.28	0.0857	3.3	M
	80	GcL(2)D$_2$M$_4$m_3		59.62	0.0070	0.0071	1.99	3.55	0.28	0.0857	3.3	M

The overlap length of 12 cm, which was selected based on the usual field practice recommendation for wrapping of RC members with composite fabrics [27], proved to be insufficient for the 1 and 2 cords/cm density SRG jackets (see Table 2, Group B, No. 17-28 specimens) as it mainly led to the debonding failure mode. The use of 36 cm overlap length in one-layered 1, 1.57, 2 cords/cm density SRG jackets in general led to the rupture of steel fabric (desirable failure mode), while in case of the 4.72 cords/cm density fabric debonding was the dominant mode of failure (see Table 2, Groups A, C, D, E, F, G). The two-layered 1 and 1.57 cords/cm SRG jackets failed due to the rupture of fabric for an overlap length of 24 cm (see Table 2, Groups E-G). For the same overlap length, however, the two-layered 4.72 cords/cm density SRG jackets exhibited a mixed mode of failure (see Table 2, Groups F, G). It should be noted that the 9.06 cords/cm density SRG jackets failed due to debonding. The main reason for that was the difficulty of the cementitious material to penetrate the very dense fabric (gap between cords was only 1.10 mm). Hence, the application of fabrics with a very high density seems to be impractical for SRG jackets.

4.2 Confinement ratio

The mechanical effects of Steel-Reinforced Grout (SRG) jacketing on concrete are in general similar to those resulting from other passive confinement systems such as stirrups or Fiber-Reinforced Polymer (FRP) jackets. The SRG jacket is mobilized in tension as a result of the lateral expansion of concrete under significant axial compressive stress. The uniformly distributed lateral confining pressure provided by the SRG jacket, σ_{lat}, around the circumference is balanced by a uniform radial pressure which reacts against the concrete lateral expansion. Restraining concrete dilation results in deformation capacity enhancement of the confined concrete. Using the deformation compatibility between the SRG jacket and the concrete surface, the lateral confining pressure, σ_{lat}, can be expressed as a function of the transverse effective strain, $\varepsilon_{s,eff}$, corresponding to either the transverse strain reached at rupture of the steel reinforced fabric, $\varepsilon_{s,rupt}$, or the transverse strain at debonding failure of the jacket layer, $\varepsilon_{s,deb}$, over the lap length, L_b [23]. The debonding strain $\varepsilon_{s,deb}$ is also influenced by both the characteristics of the mortar (interfacial bond stress) and the thickness of the fabric [23]. It should be noted that the mortar is the weakest link in the composite system, which can lead to a brittle mode of failure when the ultimate shear strength (bond stress), f_{mb}, is reached [23].

Therefore, the SRG confinement is considered successful when rupture of the fabric occurs before mortar reaches its ultimate shear strength.

In this study, using the developed experimental databank, the confinement ratio, σ_{lat}/f_{co}, was estimated for those specimens that failed due to rupture of the fabric (see Table 2):

$$\frac{\sigma_{lat}}{f_{co}} = \frac{1}{2} \cdot \frac{\rho_{SRG} E_f}{f_{co}} \varepsilon_{s,rupt} = \frac{1}{2} \cdot \overline{\rho}_{SRG} \cdot \varepsilon_{s,rupt} \tag{1}$$

In the above equation, $\rho_{SRG}=4 \cdot t_{eq}/D$ is the volumetric ratio of the SRG jacket, while t_{eq} is the equivalent thickness of the steel fabric and D represents the diameter of the cylindrical column. E_f is the modulus of elasticity of the textile, f_{co} is the compressive strength of the unconfined concrete and $\overline{\rho}_{SRG}$ is the dimensionless mechanical reinforcement ratio. Finally, $\varepsilon_{s,rupt}$ is the hoop rupture strain of the SRG jacket which is directly related to the confinement ratio (see Eq. 1). It should be mentioned that the equivalent thickness per unit width for a single layer of steel fabric used in the current database, t_{eq}, was 0.062, 0.084, 0.124, 0.254 and 0.562 mm for 1, 1.57, 2, 4.72 and 9.06 cords/cm, respectively. The modulus of elasticity, E_f, was also 110, 120, 190 GPa for 12X, 3X2, 3X2* textiles, respectively.

The ratio of the hoop strain at which rupture of the fabric occurs, $\varepsilon_{s,rupt}$, over the ultimate strain capacity of the steel fabric, $\varepsilon_{fu,s}$, represents the strain efficiency factor $k_\varepsilon(=\varepsilon_{s,rupt}/\varepsilon_{fu,s})$. The strain efficiency factor is a key parameter for assessing the confinement effectiveness of composite systems. Lam and Teng [28] reported a strain efficiency factor $k_\varepsilon=0.60$ for Fiber-Reinforced Polymer (FRP) confinement. Recent comprehensive studies on FRP concrete confinement have demonstrated the influence of concrete strength and FRP material on the hoop rupture strain [29, 30]. After the statistical processing of a large database by Ozbakkaloglu and Lim [29], an expression has been derived where the strain efficiency factor, k_ε, is related to the unconfined concrete compressive strength and the elastic modulus of fiber material. In another relevant study, Napoli and Realfonzo [31] studied experimentally the behaviour of Steel-Reinforced Polymer (SRP) confined concrete using UHTSS fabrics combined with organic matrix (resin). Based on their results, the efficiency factor k_ε equal to 0.55 was suggested for SRP systems. This implies that using steel-reinforced instead of fiber-reinforced fabrics results in a slightly lower strain efficiency factor. It should be also noted that, in general, the strain efficiency factor, k_ε, receives lower values in the FRCM systems as compared to the FRP systems mainly due to the presence of the cracks development in the mortar matrix [21, 32].

In a more recent study, Ombres and Mazzuca [33] published an experimental database covering all available studies on concrete confinement with various FRCM systems. It is noted that some of the presented experimental studies provided information on the measured k_ε values. Using this database, the average value of k_ε was estimated to be 0.33 for the studies where carbon, glass, PBO fabrics as well as hybrid fabrics made of basalt fibers, alkaline resistant (AR) glass fibers and polyvinyl alcohol (PVA) fibers were combined with inorganic matrix.

Considering the limited experimental data currently available for SRG jacketing systems, the estimation of the k_ε value for these systems should mainly rely on the previous studies on SRP-confined concrete as well as concrete confined with other FRCM systems. In the approach followed herein, the k_ε value for the SRG jacketing system is defined as the average value of the k_ε values corresponding to the SRP [31] and FRCM [33] jacketing systems, which is equal to 0.44. While more accurate values can be obtained based on lateral strain measurements, in the absence of such data, this value should provide a reasonable representative of strain efficiency factor k_ε for SRG confined concrete.

4.3 Stress-strain curves

The typical axial stress-axial strain behaviour of SRG confined cylinders subjected to monotonic compression can be characterized as a tri-linear curve [23]. In general, the first part of the curve comprises an ascending branch having the same inclination as that of the unconfined concrete. The second part is nearly linear with or without inclination (positive or negative), whereas the third part usually corresponds to a descending branch with a constant slope denoting failure of the jacket.

Fig. 4 shows the representative stress–strain curves of the SRG confined concrete cylinders that failed due to rupture of the fabric obtained from the developed experimental database (see Table 2). The axial stress, f_c, and strain, ε_c, values have been normalized to the compressive strength, f_{co}, and the corresponding strain, ε_{co}(=0.002), of the unconfined concrete, respectively. It is observed that the behaviour of SRG confined cylinders changes from brittle (Fig. 4 (a)) to semi-ductile (Fig 4 (b)) and ductile (Fig. 4 (c)), based on the level of stiffness confinement provided by the SRG jacket (i.e. equivalent thickness of the steel fabric and number of layers). To characterise this behaviour, the confinement ratio (as defined in Eq. (1)) can be rewritten as a function of the confinement stiffness ratio, ρ_K, and the strain ratio, ρ_ε, as introduced by Teng et al. [34]:

$$\frac{\sigma_{lat}}{f_{co}} = \left(\frac{1}{2}\cdot\bar{\rho}_{SRG}\cdot\varepsilon_{co}\right)\left(\frac{\varepsilon_{s,rupt}}{\varepsilon_{co}}\right) = \rho_K\cdot\rho_\varepsilon \tag{2}$$

The confinement stiffness ratio, ρ_K, is directly related to the dimensionless mechanical reinforcement ratio $\bar{\rho}_{SRG}$. The strain ratio, ρ_ε, has been estimated by assuming that $\varepsilon_{s,rupt}$=(0.44· $\varepsilon_{fu,s}$) and ε_{co}=0.002.

The confinement stiffness ratio, ρ_K, can be used as a key parameter to identify the three different types of general stress-strain behaviour corresponding to brittle, semi-ductile and ductile SRG confined concrete specimens as shown in Fig. 4. Type I curves correspond to ρ_K values lower than 0.0075 (Fig. 4(a)). The response in this case can be characterized as brittle, since as soon as the peak strength was reached an abrupt drop in the stress–strain curve was observed. For this type of specimens, compressive strength was increased by an average value of 36% while the average strain ratio, $\varepsilon_{ccu}/\varepsilon_{co}$, was equal to 1.93. For Type II curves, ρ_K ranged between 0.0075 and 0.014 (Fig. 4(b)). The response can be characterized as semi-ductile with limited strain ductility. For these specimens, the average increase in the compressive strength was between 32 and 51%, whereas the average values of $\varepsilon_{ccu}/\varepsilon_{co}$ were between 2.58 and 3.50. As observed in Fig. 4(b), the compressive strength did not increase after yielding (Fig. 4(b)). Finally, Type III curves correspond to ρ_K ranging between 0.014 and 0.141 (Fig. 4(c)). The stress-strain response in this case can be characterized as ductile with a post-yield hardening branch in most cases. The only exception is specimen GcL(1)$D_4M_4\ell$_1 (ρ_K=0.0143) which presented a post-yield descending branch. However, this specimen reached high ultimate strain values and therefore can be considered as ductile (Fig. 4(c)). The average increase in the compressive strength ranged between 35 to 150%, while the $\varepsilon_{ccu}/\varepsilon_{co}$ received values between 3.23 and 7.03. The lower limit of $\varepsilon_{ccu}/\varepsilon_{co}$(=3.23) corresponds to specimen GcL(2)D_2M_4m_3 (ρ_K=0.0857), which despite the fact that the strength increased significantly (high inclination in the post-yield hardening branch), the ultimate strain capacity was not reached due to the mixed mode of failure (see Fig. 3(b)).

For better comparison, the three typical stress-strain curves (brittle, semi-ductile and ductile) of SRG confined concrete are illustrated in Fig. 5 using the ρ_K limits discussed above.

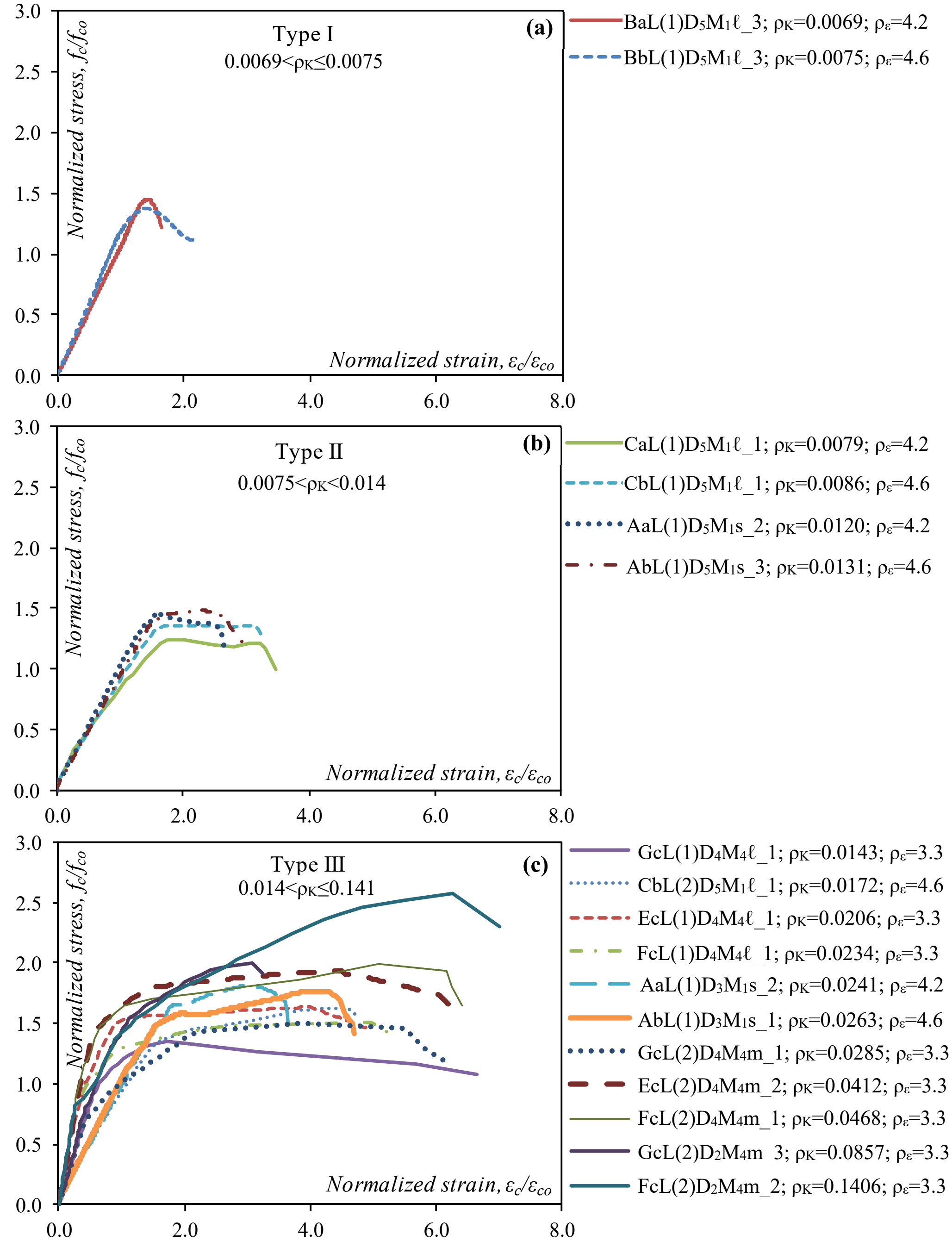

Figure 4: Axial stress-strain curves for SRG confined concrete cylinders

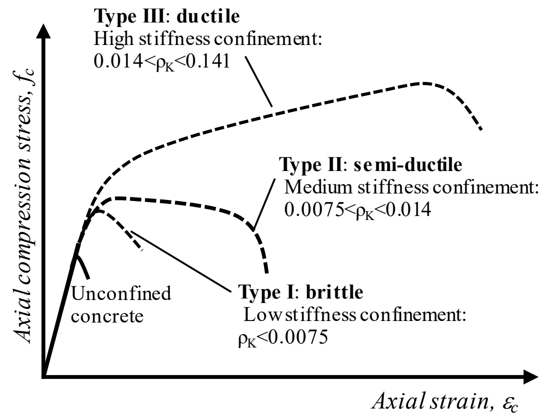

Figure 5: Typical stress-strain responses for SRG confined concrete cylinders

4.4 SRG confined concrete compressive strength and axial strain

The effect of SRG jacketing on the compressive strength and ultimate strain of confined concrete specimens is evaluated by estimating the ratios f_{cc}/f_{co} and $\varepsilon_{ccu}/\varepsilon_{co}$, respectively, as presented in Table 2. The variation in the adopted SRG jacketing schemes (i.e. density of the fabric, number of layers, modulus of elasticity and the concrete grade) is reflected through the values received by the dimensionless mechanical reinforcement ratio, $\bar{\rho}_{SRG}$. f_{cc}/f_{co} and $\varepsilon_{ccu}/\varepsilon_{co}$ are plotted against $\bar{\rho}_{SRG}$ for all the test specimens in Figs. 6(a), (b). The higher values of $\bar{\rho}_{SRG}$ correspond to the cases with denser steel fabrics, more than one layer of jackets and lower concrete grade. As observed in Figs. 6(a) and (b), the f_{cc}/f_{co} and $\varepsilon_{ccu}/\varepsilon_{co}$ ratios increase as SRG-confined concrete increases for the SRG confined specimens that failed due to the rupture of steel fabric or exhibited a mixed mode of failure. This trend is not observed for the specimens that failed due to debonding especially for the higher $\bar{\rho}_{SRG}$ values.

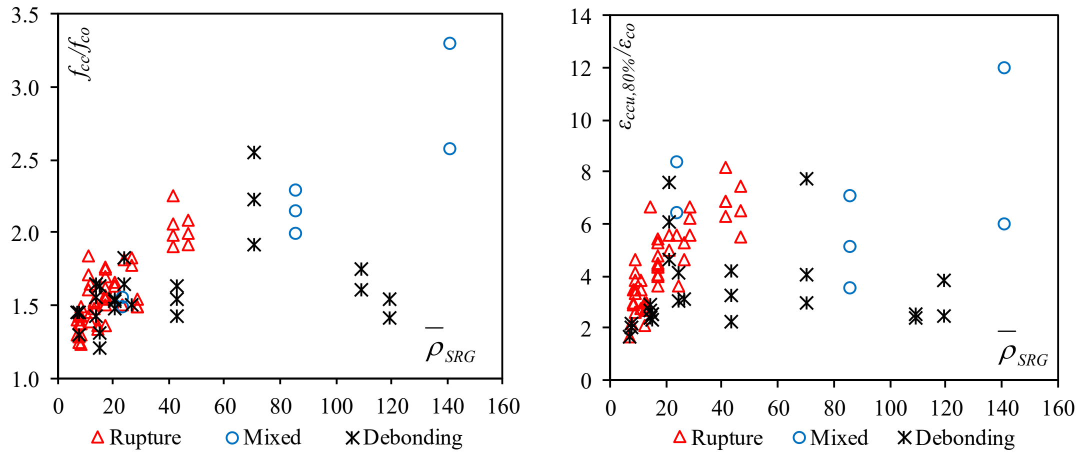

Figure 6: (a) Strength confinement ratio, f_{cc}/f_{co}, and (b) strain ratio, $\varepsilon_{ccu}/\varepsilon_{co}$, versus the dimensionless mechanical reinforcement ratio, $\bar{\rho}_{SRG}$, for specimens of the database

For those specimens that failed due to the rupture of steel fabric, a detailed representation of the variation of f_{cc}/f_{co} and $\varepsilon_{ccu}/\varepsilon_{co}$ with SRG-confined concrete is plotted in Figs. 7(a) and (b), respectively. The comparison made between specimens having the same SRG jacket (i.e. density, type of fabric and number of layers, see legend of Fig. 7) indicates that in general the effectiveness of SRG jacket increases as the unconfined concrete strength decreases. This conclusion is in accordance with the observations made for FRP and TRM jacketing systems (e.g. [17, 35]).

For those specimens that rupture of the steel fabric was the dominant mode of failure, one-layered SRG jackets could increase the average strength capacity of the unconfined concrete by 44%, 50%, and 80% for 1, 1.57 and 2 cords/cm steel fabrics, respectively. By adding the second layer of SRG jackets, these numbers were increased to 59% and 87% for 1 and 1.57 cords/cm steel fabrics, respectively. In the case of one-layered SRG jackets with fabric density of 4.72 cords/cm, where debonding was observed, the average strength capacity of the unconfined specimens was increased by 88%. Adding the second layer of SRG jackets increased further the strength capacity of the unconfined specimens by 31%, and changed the dominant failure mode to the mixed mode of failure. Similarly, one-layered SRG jackets improved the ultimate strain of the unconfined specimens by 307%, 570%, and 452% for 1, 1.57 and 2 cords/cm steel fabrics, respectively. Using two-layered SRG jackets increased the ultimate strain of the unconfined specimens by 46% and 16% for 1 and 1.57 cords/cm steel fabrics, respectively. Finally, the two-layered 4.72 cords/cm jackets improved the ultimate strain of the unconfined specimens by 676% and led to the mixed mode of failure.

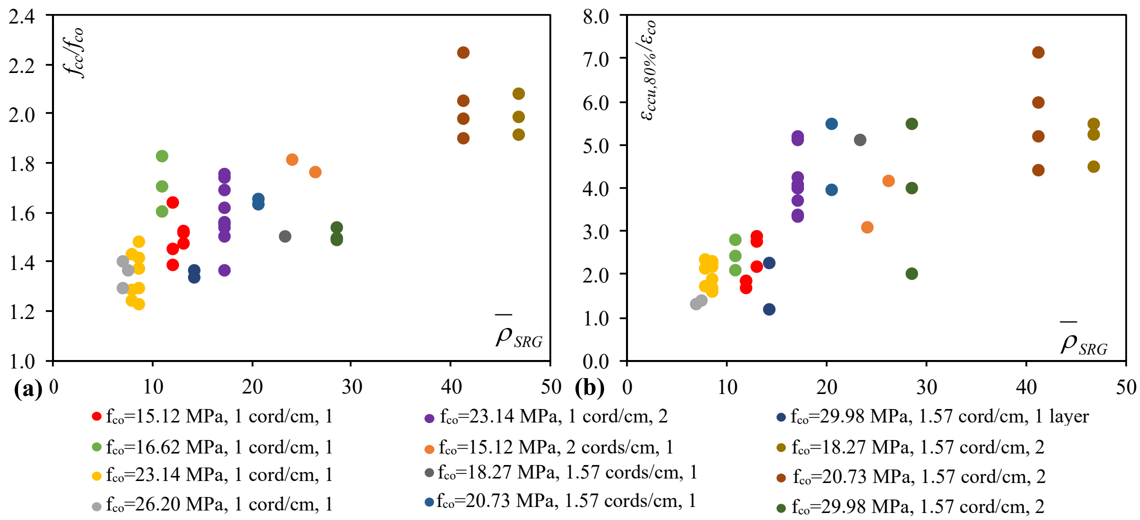

Figure 7: (a) Strength confinement ratio, f_{cc}/f_{co}, and (b) strain ratio, $\varepsilon_{ccu}/\varepsilon_{co}$, versus the dimensionless mechanical reinforcement ratio, $\bar{\rho}_{SRG}$, for specimens of the database that failed due to rupture of the fabric

The data from the developed experimental database indicates that the type of mortar did not considerably influence the strength and deformation capacity of the specimens when the failure mode was due to the rupture of steel fabric. However, the improvement in the compressive strength and the ultimate strain of unconfined concrete is slightly higher when a mortar with higher flexural strength is utilized.

5. Existing confinement models

5.1 Compressive strength and ultimate strain

The passive confinement either provided by more traditional (e.g. steel) or innovative materials (e.g. composite materials) can modify substantially the mechanical characteristics of concrete. In the past two decades, a wide range of confinement models have been proposed, the majority of which relate the confined strength, f_{cc}, and ultimate strain, ε_{ccu}, to the lateral confining stress, σ_{lat}, using the following general equations [27, 36]:

$$\frac{f_{cc}}{f_{co}} = 1 + \kappa \cdot \left(\frac{\sigma_{lat}^{\beta}}{f_{co}} \right)^{\alpha} \tag{3}$$

$$\frac{\varepsilon_{ccu}}{\varepsilon_{co}} = \mu + \frac{\lambda}{\varepsilon_{co}} \cdot \left(\frac{\sigma_{lat}^{\delta}}{f_{co}} \right)^{\gamma} \tag{4}$$

where f_{co} is the compressive strength of the unconfined concrete, and σ_{lat} is the lateral confining pressure exerted by the jacketing system applied. α, β, γ, δ, κ, λ are empirical constant parameters and μ is the normalized ultimate strain of unconfined concrete.

In this study, eight existing models for predicting the compressive strength of confined concrete were selected from literature (see Table 3). The first three models in Table 3 are code-based models generally used for FRP concrete confinement. The model proposed by the Italian guidelines [37] considers a nonlinear relationship between the confinement pressure and the plain concrete strength. The ACI 440 [38] model is originally based on the model proposed by Lam and Teng [28], and is also adopted by ACI 549.4R-13 [39] for FRCM confinement. The TR55 model [40] is based upon the work of Teng et al. [34], where the strength increase due to confinement is related to the non-dimensional stiffness ratio, ρ_{κ}, and the strain ratio, ρ_{ε}. The rest of the models were obtained from regression analyses performed on the results of axial compression tests on concrete specimens confined using different FRCM jacketing systems. Triantafillou et al. [17] and Ombres [21] confinement models were proposed for TRM- and

PBO-confined concrete, respectively. Thermou et al. [23] model was developed based on the results of SRG-confined concrete specimens, while the model suggested by Napoli and Realfonzo [31] was related to the steel-reinforced polymer (SRP) jacketing system. The last model was recently proposed by Ombres and Mazzuca [33] for FRCM-confined concrete, which includes TRM (carbon, glass, basalt fabrics), PBO, and SRG systems.

Table 3. Confinement models for concrete cylinders

Confinement models	Expressions for f_{cc}/f_{co} and $\varepsilon_{ccu}/\varepsilon_{co}$
CNR-DT 200 [37]	$f_{cc}/f_{co} = 1 + 2.6 \cdot \left(\sigma_{lat}/f_{co}\right)^{0.67}$; $\varepsilon_{ccu}/\varepsilon_{co} = 1.75 + 0.75\left(\sigma_{lat}/f_{co}\right)^{0.5}$
ACI Model [38, 39]	$f_{cc}/f_{co} = 1 + 3.1\left(\sigma_{lat}/f_{co}\right)$; $\varepsilon_{ccu}/\varepsilon_{co} = 1.5 + 12\left(\sigma_{lat}/f_{co}\right)\left(\varepsilon_{s,rupt}/\varepsilon_{co}\right)^{0.45}$
TR55 [40]	$f_{cc}/f_{co} = 1 + 5.25 \cdot \left(\rho_K - 0.01\right)\rho_\varepsilon$; if $\rho_K \geq 0.01$ $f_{cc}/f_{co} = 1$; if $\rho_K < 0.01$; $\varepsilon_{ccu}/\varepsilon_{co} = 1.75 + 6.5 \cdot \rho_K^{0.8} \cdot \rho_\varepsilon^{1.45}$
Triantafillou et al. [17]	$f_{cc}/f_{co} = 1 + 1.9 \cdot \left(\sigma_{lat}/f_{co}\right)$; $\varepsilon_{ccu}/\varepsilon_{co} = 1 + \left(0.047/\varepsilon_{co}\right) \cdot \left(\sigma_{lat}/f_{co}\right)$
Ombres [21]	$f_{cc}/f_{co} = 1 + 5.268 \cdot \sigma_{lat}/f_{co}$; $\varepsilon_{ccu}/\varepsilon_{co} = \left(0.041/\varepsilon_{co}\right) \cdot \left(\sigma_{lat}/f_{co}\right)^{0.25} - 1.02$
Thermou et al. [23]	$f_{cc}/f_{co} = 1 + 3.7\,\sigma_{lat}/f_{co}$; $\varepsilon_{ccu}/\varepsilon_{co} = 1 + \left(0.027/\varepsilon_{co}\right) \cdot \left(\sigma_{lat}/f_{co}\right)$
Napoli & Realfonzo [31]	$f_{cc}/f_{co} = 1 + 4.21\left(\sigma_{lat}/f_{co}\right)$; $\varepsilon_{ccu}/\varepsilon_{co} = 1.75 + 22.97\left(\sigma_{lat}/f_{co}\right)^{0.64}$
Ombres & Mazzuca [33]	$f_{cc}/f_{co} = 1 + 0.913\left(\sigma_{lat}/f_{co}\right)^{0.5}$; $\varepsilon_{ccu}/\varepsilon_{co} = 1 + 0.963\left(\sigma_{lat}/f_{co}\right) \cdot \left(\varepsilon_{s,rupt}/\varepsilon_{co}\right)^{0.5}$

The confinement models listed in Table 3 were utilized to estimate the confined strength and ultimate strain of the specimens that failed due to the rupture of steel fabric (Table 2). The diagrams in Figs. 8, 9 illustrate how the predicted values of $(f_{cc}/f_{co})^{anal}$ and $(\varepsilon_{ccu}/\varepsilon_{co})^{anal}$ are compared to the experimental values of $(f_{cc}/f_{co})^{exp}$ and $(\varepsilon_{ccu}/\varepsilon_{co})^{exp}$. For the specimens that are close to the 45^{o} linear line, the selected confinement model provides an accurate prediction of the confined strength. If the predicted values lie above or below the 45^{o} line, however, it means that the selected confinement model has led to underestimated or overestimated results, respectively. According to Fig. 8, in general, the strength prediction models examined in this study underestimate the SRG confined concrete strength. This is also the case for the majority of the ultimate strain prediction models except those of Ombres [21] and Napoli and Realfonzo [31] where the predicted ultimate strain is generally overestimated (Fig. 9).

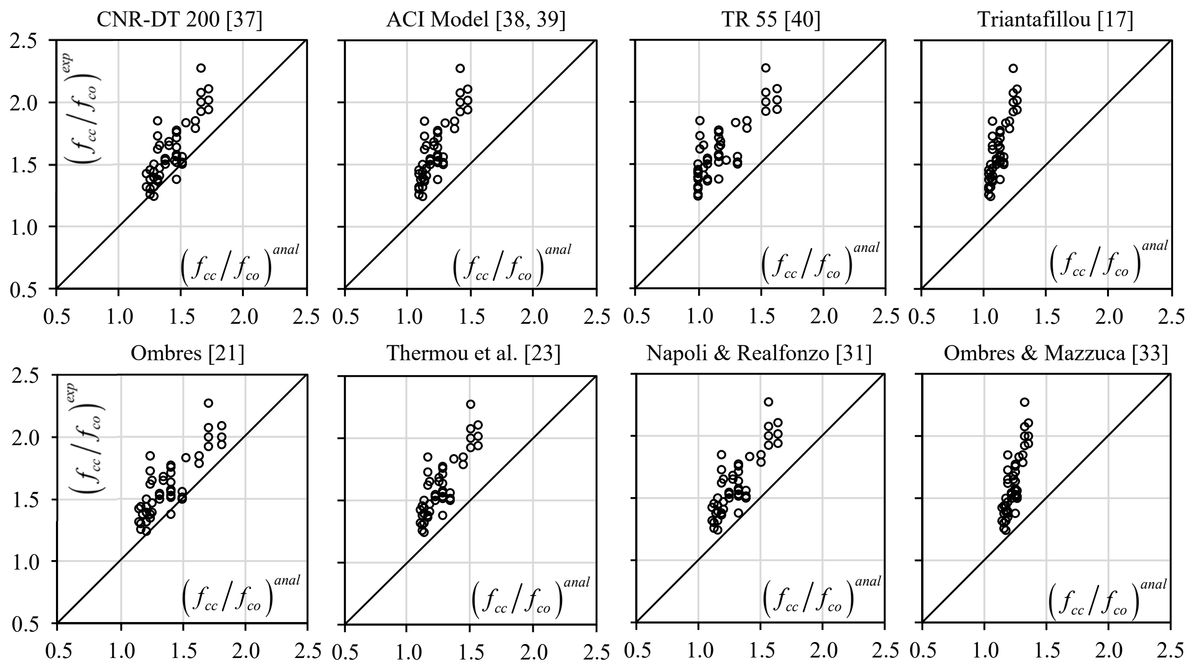

Figure 8: Assessment of the compressive strength using existing concrete confinement models for the specimens that failed due to the rupture of steel fabric from the experimental database

5.2 Accuracy of the predicted confined strengths and ultimate strains

The accuracy of the confinement models presented in Table 3 for predicting the experimental values of the SRG confined concrete strength, f_{cc}, and ultimate strain, ε_{ccu}, were assessed by the help of statistical indices. The objective was to identify the most adequate confinement models for SRG confinement. It is recalled that from the experimental data only those specimens that failed due to the rupture of steel fabric were considered. The Average Absolute Error (AAE), the Mean Square Error (MSE) and the Standard Deviation (SD) indices corresponding to each confinement model were calculated as follows:

$$AAE = \frac{\sum_{i=1}^{N} \left| \frac{(x)_i^{anal} - (x)_i^{\exp}}{(x)_i^{\exp}} \right|}{N} \quad (5)$$

$$MSE = \frac{\sum_{i=1}^{N}\left[(x)_i^{anal} - (x)_i^{\exp}\right]^2}{N} \tag{6}$$

$$SD = \sqrt{\frac{\sum_{i=1}^{N}\left[(x)_i^{anal} / (x)_i^{\exp} - (x)_{avg}^{anal} / (x)_{avg}^{\exp}\right]^2}{N-1}} \tag{7}$$

where $(x)_i^{anal}$ represents the predicted values of concrete confined strength ratio, $(f_{cc}/f_{co})^{anal}$, and ultimate strain ratio, $(\varepsilon_{ccu}/\varepsilon_{co})^{anal}$. Similarly, $(x)_i^{exp}$ shows the experimental values of concrete confined strength ratio, $(f_{cc}/f_{co})^{exp}$, and ultimate strain ratio $(\varepsilon_{ccu}/\varepsilon_{co})^{exp}$. N is the total number of specimens corresponding to the SRG confined cylinders failed due to the rupture of steel fabric (here 48). The subscript "avg" indicates the average value.

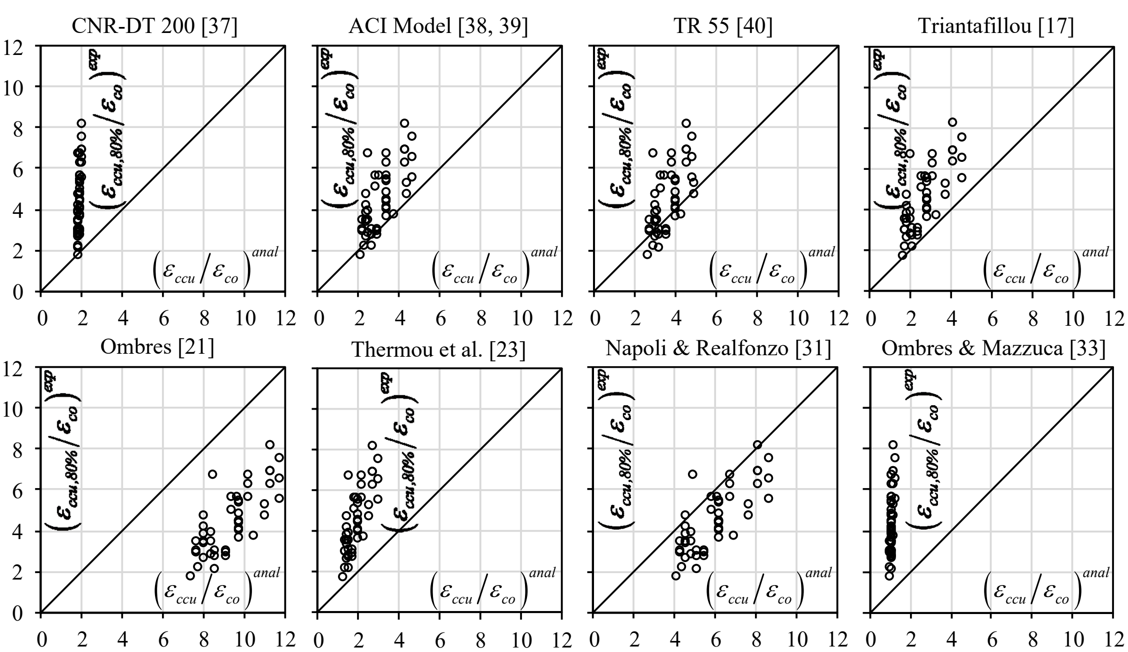

Figure 9: Assessment of the ultimate strain using existing concrete confinement models for the specimens that failed due to the rupture of steel fabric from the experimental database

The calculated AAE, MSE and SD values for the selected confinement models are listed in Table 4. In general, the accuracy of the models was better for the prediction of the concrete confined strength rather than the ultimate strain, while none of the models could accurately predict both f_{cc}/f_{co} and $\varepsilon_{ccu}/\varepsilon_{co}$ values. Based on the results, CNR-DT 200 [37] and Ombres [21] models provided the most accurate predictions of the f_{cc}/f_{co} with the minimum AAE and MSE values compared to the other models. However, these models were not very accurate in predicting the $\varepsilon_{ccu}/\varepsilon_{co}$ values. This was especially evident for Ombres [21] model, which led to over 135% AAE. On the other hand, it is shown in Table 4 that TR55 [40] and ACI [38, 39] models provided the most accurate results for $\varepsilon_{ccu}/\varepsilon_{co}$. It should be noted that using the average plus standard deviation of the predicted to the experimental values also leads to the same conclusions.

Table 4. Statistical indices

Confinement models	f_{cc}/f_{co}			$\varepsilon_{ccu}/\varepsilon_{co}$		
	AAE (%)	MSE	SD	AAE (%)	MSE	SD
CNR-DT 200 [37]	9.27	0.042	0.077	50.57	8.489	0.186
ACI Model [38, 39]	21.83	0.154	0.067	26.44	2.884	0.202
TR55 [40]	25.27	0.182	0.070	22.96	1.986	0.264
Triantafillou et al. [17]	27.21	0.235	0.073	34.53	3.855	0.157
Ombres [21]	12.30	0.057	0.071	135.60	63.574	0.700
Thermou et al. [23]	19.14	0.120	0.066	51.33	7.315	0.123
Napoli & Realfonzo [31]	16.85	0.096	0.067	47.22	3.561	0.375
Ombres & Mazzuca [33]	20.68	0.158	0.086	70.94	13.121	0.103
Proposed model	6.03	0.019	0.079	19.50	1.036	0.244

6. New confinement model for SRG jacketing

It was discussed in the previous sections that the confinement stiffness ratio, ρ_K, and the strain ratio, ρ_ε, play key roles in the confined concrete compressive strength and the ultimate strain of SRG-confined concrete specimens. Therefore, the following general equations are adopted in this study to obtain a new confinement model for SRG-confined concrete:

$$f_{cc}/f_{co} = 1 + f_\sigma(\rho_K) \cdot \rho_\varepsilon \tag{8}$$

$$\varepsilon_{ccu}/\varepsilon_{co} = 1.75 + f_\varepsilon(\rho_K) \cdot \rho_\varepsilon \tag{9}$$

where f_{cc} and f_{co} are the compressive strength of unconfined and confined concrete, respectively. ε_{ccu} is the ultimate strain of confined concrete and ε_{co} is the strain corresponding to the peak compressive strength of unconfined concrete. ρ_K and ρ_ε are the confinement stiffness ratio and strain ratio, respectively. $f_\sigma(\rho_K)$ and $f_\varepsilon(\rho_K)$ are functions of ρ_K. The constant 1.75 in Equation (9) implies that the ultimate strain of unconfined concrete is considered to be equal to $\varepsilon_{cu}=\varepsilon_{co}\times1.75=0.002\times1.75=0.0035$, which is the value adopted for unconfined concrete by most design guidelines [e.g. 41]. It should be noted that, in case of FRP-confined concrete, a simple expression has been proposed by Lim and Ozbakkaloglu [8, 9], which represents the $\varepsilon_{cu}/\varepsilon_{co}$ ratio as a function of f_{co} to provide a more accurate estimation of the ultimate strain. Generalized equations similar to Eqs. (8) and (9) have been also proposed by other researchers (e.g. [8-9, 34, 42-44]) to represent confinement models for FRP-confined concrete.

The database developed in this study is used for obtaining the best fit linear equations for $f_\sigma(\rho_K)$ and $f_\varepsilon(\rho_K)$ functions corresponding to the SRG-confined concrete cylinders failed due to the rupture of steel fabric. Based on the results, the following equations are proposed to estimate the confined strength and the ultimate axial strain of SRG-confined concrete:

$$f_{cc}/f_{co} = 1+\left(5.73\cdot\rho_K+0.03\right)\rho_\varepsilon \tag{10}$$

$$\varepsilon_{ccu}/\varepsilon_{co} = 1.75+32.78\cdot\rho_K\cdot\rho_\varepsilon \tag{11}$$

where f_{cc} and f_{co} are the compressive strength of confined and unconfined concrete, respectively, ε_{ccu} is the ultimate strain of confined concrete, ε_{co} is the strain at the peak compressive strength of unconfined concrete, $\varepsilon_{s,rupt}(=0.44\times\varepsilon_{fu,s})$ is the hoop rupture strain of the SRG jacket, $\varepsilon_{fu,s}$ is the ultimate strain capacity of the steel fabric, ρ_K is the confinement stiffness ratio (here ranging between 0.007 and 0.047), and ρ_ε is the strain ratio.

The predicted values of $(f_{cc}/f_{co})^{anal}$ and $(\varepsilon_{ccu}/\varepsilon_{co})^{anal}$ based on the proposed confinement model are compared with the experimental values of $(f_{cc}/f_{co})^{exp}$ and $(\varepsilon_{ccu}/\varepsilon_{co})^{exp}$ in Figs 10(a) and (b). It is shown in Table 4 that the AAE, MSE and AAE+SD statistical indices corresponding to the new model are considerably lower (up to 98% less) than those of existing models developed for FRCM-confined concrete. It can be seen that Equations (10) and (11) accurately predicted the SRG-confined concrete strength and ultimate strain values leading to 6.0% and 19.5% AAE, respectively. This implies that the proposed confinement model can be efficiently used to estimate the strength and the ultimate strain of SRG-confined columns for practical design purposes.

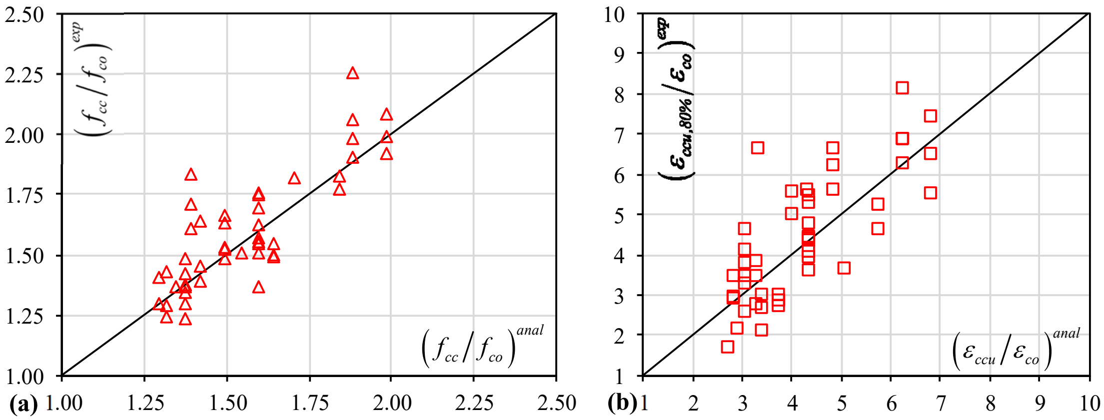

Figure 10: Assessment of the confined strength and ultimate strain using the new concrete confinement model based on the specimens that failed due to rupture from the experimental database

7. Summary and conclusions

Considering the lack of available information on the newly developed Steel-Reinforced Grout (SRG) retrofitting technique, this study aimed to investigate the axial stress–strain response of concrete confined with SRG jackets comprising of Ultra-High Tensile Strength Steel textiles embedded in an inorganic binder. A comprehensive experimental database was compiled based on all existing tests on SRG-confined concrete subjected to monotonic uniaxial compression. The results were then critically analysed to identify the influence of key design parameters and develop design-oriented confinement models. The main conclusions drawn are as follows:

- The SRG confinement is considered successful when rupture of the fabric occurs before mortar reaches its ultimate shear strength. For one-layered SRG jackets, using 36 cm overlap length generally led to the rupture of steel fabric and therefore considered to be adequate. While the overlap length of 24 cm was sufficient for two-layered SRG jackets with low- to medium-density fabrics (1 to 2 cords/cm), in the case of 4.72 cords/cm density textiles it resulted in a mixed mode of failure. SRG jackets with very high-density fabrics (9.06 cords/cm) failed due to debonding (unfavourable failure mode) and were shown to be impractical due to the difficulties in the wrapping process and penetration of mortar through the small spacing between the cords.

- Similar to the observations made for FRP and TRM jacketing systems, it was shown that in general the effectiveness of SRG jacket increases as the unconfined concrete strength decreases. For the specimens that failed due to the rupture of steel fabric or exhibited a mixed failure mode, the confinement strength, f_{cc}, and the ultimate strain, ε_{ccu}, increased by increasing the dimensionless mechanical reinforcement ratio, $\bar{\rho}_{SRG}$, while the type of mortar did not considerably influence the results.
- The axial stress–strain response of SRG-confined concrete is greatly affected by the confinement stiffness ratio, ρ_K, where a brittle, semi-ductile and ductile behaviour is generally observed for $\rho_K<0.0075$, $0.0075<\rho_K<0.014$ and $\rho_K>0.014$, respectively.
- None of the existing confinement models for FRP and FRCM systems could accurately predict both the strength and ultimate strain values of SRG confined concrete. Using the experimental database developed in this study, a new confinement model was proposed for SRG-confined concrete as a function of the confinement stiffness ratio, ρ_K, and the strain ratio, ρ_ε. It was shown that the proposed model could predict the strength and ultimate strain of SRG-confined concrete with a much better accuracy compared to the existing models.

While the results of this study should prove useful for the practical design of SRG-confined columns, further experimental studies are necessary to assess the hoop strain of SRG-confined concrete and obtain more accurate values for the strain efficiency factor, k_ε. Moreover, the existing database needs to be enhanced by experimental tests that account for the effect of multiple layers of textiles with different density and for a wider range of geometric and material properties. The proposed confinement model could then be compared against a larger sample of specimens and refined if needed.

8. Acknowledgements

This project has received funding from the European Union's Horizon 2020 research and innovation programme under the Marie Skłodowska-Curie grant agreement No. 700863.

9. References

[1]. T.C. Triantafillou, N. Plevris, Strengthening of RC beams with epoxy-bonded fibre-composite materials, Mater. Struct. 25(4) (1992) 201-211.

[2]. Y-W Zhou, Y-F Wu, General model for constitutive relationships of concrete and its composite structures, Compos. Struct. 94 (2012) 580-592.

[3]. P. Li, Y-F Wu, Stress–strain model of FRP confined concrete under cyclic loading, Compos. Struct. 134 (2015) 60–71.

[4]. Y. Zhou, X. Liu, F. Xing, H. Cui, L. Sui, Axial compressive behavior of FRP-confined lightweight aggregate concrete: An experimental study and stress-strain relation model, Constr. Build. Mater. 119 (2016) 1–15.

[5]. Y. Zhou, M. Li, L. Sui, F. Xing, Effect of sulfate attack on the stress–strain relationship of FRP-confined concrete, Constr. Build. Mater. 110 (2016) 235–250.

[6]. A. Fallah Pour, A. Gholampour, T. Ozbakkaloglu, Influence of the measurement method on axial strains of FRP-confined concrete under compression, J. Compos. Struct. 188 (2018) 415-424.

[7]. Y.-L. Bai, J.-G. Dai, T. Ozbakkaloglu, Cyclic stress-strain model incorporating buckling effect for steel reinforcing bars embedded in FRP-confined concrete, J. Compos. Struct. 182 (2017) 54-66.

[8]. J.C. Lim, T. Ozbakkaloglu, Confinement Model for FRP-Confined High-Strength Concrete, J. Compos. Constr. 18(4) (2014):04013058.

[9]. J.C. Lim, T. Ozbakkaloglu, Erratum: Confinement Model for FRP-Confined High-Strength Concrete, J. Compos. Constr. 20(6) (2016):08216001.

[10]. J.C. Lim, T. Ozbakkaloglu, Unified stress-strain model for FRP and actively confined normal-strength and high-strength concrete, J. Compos. Constr. 19(4) (2015):04014072.

[11]. J.C. Lim, T. Ozbakkaloglu, Influence of silica fume on stress-strain behavior of FRP-confined HSC, Constr. Build. Mater. 63 (2014) 11–24.

[12]. T. Vincent, T. Ozbakkaloglu, Influence of fiber orientation and specimen end condition on axial compressive behavior of FRP-confined concrete, Constr. Build. Mater. 47 (2013) 814-826.

[13]. S. Kaurtz, P. Balaguru, Comparison of inorganic and organic matrices for strengthening of RC beams with carbon sheets, J. Struct. Eng. 127(1) (2001) 35-42.

[14]. R. Garon, P.N. Balaguru, H. Toutanji, Performance of inorganic polymer-fiber composites for strengthening and rehabilitation of concrete beams, FRPRCS-5 Conf, Burgoyne, C J, ed, Thomas Telford, London, Cambridge, UK, 16-18 July 2001, Vol 1, p. 53-62.

[15]. Toutanji H, Deng Y, Jia M. Fatigue performance of RC beams strengthened with cf sheets bonded by inorganic matrix. FRPRCS-6 Conf, Tan KH, ed, World Scientific Publishing Co, Singapore 8-10 July 2003, Vol 2, 875-884.

[16]. Wu HC, Teng J. Concrete confined with fiber reinforced cement based thin sheet composites. FRPRCS-6 Conf, Tan KH, ed, (2003). World Scientific Publishing Co, Singapore 8-10 July 2003, Vol 1, 591-600.

[17]. T.C. Triantafillou, C.G. Papanicolaou, P. Zissimopoulos, T. Laourdekis, Concrete confinement with textile-reinforced mortar jackets, ACI Struct. J. 103(1) (2006) 28–37.

[18]. M. Di Ludovico, A. Prota, G. Manfredi, Structural upgrade using basalt fibers for concrete confinement, J. Compos. Constr. 14(5) (2010) 541–552.

[19]. A. D'Ambrisi, L. Feo, F. Focacci, Bond-slip relations for PBO-FRCM materials externally bonded to concrete, J. Compos. B Eng. 43(8) (2012) 2938-2949.

[20]. F. De Caso y Basalo, F. Matta, A. Nanni, Fiber-reinforced cement-based composite system for concrete confinement, Constr. Build. Mater. 32 (2012) 55–65.

[21]. L. Ombres, Concrete confinement with a cement-based high-strength composite material, Compos. Struct. 109 (2014) 294–304.

[22]. G.E. Thermou, S.J. Pantazopoulou, Metallic fabric jackets: an innovative method for seismic retrofitting of substandard RC prismatic members, fib Struct. Concr. J. 8(1) (2007) 35-46.

[23]. G.E. Thermou, K. Katakalos, G. Manos, Concrete confinement with steel-reinforced grout jackets, Mater. Struct. 48(5) (2015) 1355-1376.

[24]. G.E. Thermou, K. Katakalos, G. Manos, Influence of the cross section shape on the behaviour of SRG-confined prismatic concrete specimens, Mater. Struct. 49(3) (2016) 869-887.

[25]. G.E. Thermou, K. Katakalos, G. Manos, Influence of the loading rate on the axial compressive behavior of concrete specimens confined with SRG jackets, ECCOMAS Thematic Conference COMPDYN, Greece, Kos, Paper No. 1482, 2013.

[26]. G.E. Thermou, I. Hajirasouliha, Compressive behaviour of concrete columns confined with Steel-Reinforced Grout jackets, Comp. Part B: Eng. 138 (2018) 222-231.

[27]. fib Bulletin 14, Externally bonded FRP reinforcement for RC structures, Report by Task group 9.3, fédération internationale du béton (fib), Lausanne, Switzerland, 2001.

[28]. L. Lam, J.G. Teng, Design-oriented stress-strain model for FRP-confined concrete, Constr. Build. Mater. 17(6–7) (2003) 471–489.

[29]. T. Ozbakkaloglu, J.C. Lim, Axial compressive behavior of FRP-confined concrete: Experimental test database and a new design-oriented model, J. Compos. B Eng. 55 (2013) 607–634.

[30]. J.C. Lim, T. Ozbakkaloglu, Hoop strains in FRP-confined concrete columns: experimental observations, Mater. Struct. 48 (2015) 2839-2854.

[31]. A. Napoli, R. Realfonzo, Compressive behavior of concrete confined by SRP wraps, Constr. Build. Mater. 127 (2016) 993-1008.

[32]. T. Trapko, Confined concrete elements with PBO-FRCM composites, Constr. Build. Mater. 73 (2014) 332–338.

[33]. L. Ombres, S. Mazzuca, Confined concrete elements with cement-based composites: confinement effectiveness and prediction models, J. Compos. Constr. 21(3) (2017) Article number 04016103.

[34]. J.G. Teng, T. Jiang, L. Lam, Y.Z. Luo, Refinement of a design-oriented stress–strain model for FRP-confined concrete, J. Compos. Constr. 13(4) (2009) 269–278.

[35]. R. Realfonzo, A. Napoli, Concrete confined by FRP systems: confinement efficiency and design strength models, J Compos B: Eng 42(4) (2011) 736–755.

[36]. T. Ozbakkaloglu, J.C. Lim, T. Vincent, FRP-confined concrete in circular sections: Review and assessment of stress–strain models, Eng. Struct. 49 (2013) 1068-1088.

[37]. CNR (Consiglio Nazionale Delle Ricerche), Guide for the design and construction of externally bonded FRP systems for strengthening existing structures, CNR-DT200, Italian National Research Council, Rome, Italy, 2004.

[38]. American Concrete Institute (ACI) Committee, Guide for the design and construction of externally bonded FRP systems for strengthening concrete structures, ACI 440.2R-08, Farmington Hills, MI, 2008.

[39]. ACI (American Concrete Institute), Guide to design and construction of externally bonded fabric-reinforced cementitious matrix systems for repair and strengthening concrete and masonry structures, ACI 549.4 R-13, ACI Committee 549, Farmington, MI, 2013.

[40]. Concrete Society, Design guidance for strengthening concrete structures using fibre composite materials, TR 55 Third edition, Camberley, Concrete Society, 2012.

[41]. CEN (European Committee for Standardization), Design of concrete structures - Part 1-1. Eurocode 2 (EN 1992-1-1:2004), Brussels, Belgium, 2004.

[42]. P. Sadeghian, A. Fam, Improved design-oriented confinement models for FRP-wrapped concrete cylinders based on statistical analyses, Eng Struct 87 (2015) 162–182.

[43]. R. Kumutha, R. Vaidyanathan, M.S. Palanichamy, Behaviour of reinforced concrete rectangular columns strengthened using GFRP, Cement Concr. Compos. 29(8) (2007) 609–615.

[44]. B. Keshtegara, P. Sadeghian, A. Gholampour, T. Ozbakkaloglu, Nonlinear modeling of ultimate strength and strain of FRP-confined concrete using chaos control method, J. Compos. Struct. 163 (2017) 423-431.